International Journal of Power Electronics and Drive System (IJPEDS)
Vol. 8, No. 3, September 2017, pp. 1035~1049
ISSN: 2088-8694, DOI: 10.11591/ijpeds.v8i3.pp1035-1049

Constant Switching Frequency and Torque Ripple Minimization of DTC of Induction Motor Drives with Three-level NPC Inverter

Huzainirah Ismail[1], Fazlli Patkar[2], Auzani Jidin[3], Aiman Zakwan Jidin[4], Noor Azida Noor Azlan[5], Tole Sutikno[6]
[1,2,3,5] Faculty of Electrical Engineering, Universiti Teknikal Malaysia Melaka (UTeM), Melaka, Malaysia
[4] Faculty of Engineering Technology, Universiti Teknikal Malaysia Melaka (UTeM), Melaka, Malaysia
[6] Department of Electrical Engineering, Universitas Ahmad Dahlan (UAD), Yogyakarta, Indonesia

Article Info

Article history:

Received May 13, 2017
Revised Jul 26, 2017
Accepted Aug 20, 2017

Keyword:

Direct torque control
Induction motor
Multilevel inverter
Neutral-point clamped

ABSTRACT

Direct Torque Control (DTC) is widely applied for ac motor drives as it offers high performance torque control with a simple control strategy. However, conventional DTC poses some disadvantages especially in term of variable switching frequency and large torque ripple due to the utilization of torque hysteresis controller. Other than that, performance of conventional DTC fed by two-level inverter is also restricted by the limited numbers of voltage vectors which lead to inappropriate selection of voltage vectors for different speed operations. This research aims to propose a Constant Switching Frequency (CSF) torque controller for DTC of induction motor (IM) fed by three-level Neutral-Point Clamped (NPC) inverter. The proposed torque controller utilizes PI controller which apply different gain for different speed operation. Besides, the utilization of NPC inverter provides greater number of voltage vectors which allow appropriate selection of voltage vectors for different operating condition. Using the proposed method, the improvement of DTC drives in term of producing a constant switching operation and minimizing torque ripple are achieved and validated via experimental results.

Corresponding Author:

Fazlli Patkar,
Faculty of Electrical Engineering,
Universiti Teknikal Malaysia Melaka,
Hang Tuah Jaya, 76100 Durian Tunggal, Melaka, Malaysia.
Email: fazlli@utem.edu.my

1. INTRODUCTION

Since its introduction in the mid 1980's, Direct Torque Control (DTC) has continuously receives wide acceptance for control of ac machines due to its control simplicity and fast torque dynamic response. Compared to Field Oriented Control (FOC), the high performance control of the machines is achieved without the need of current controller, frame transformations, speed sensor and knowledge of machine parameter. In order to control flux and electromagnetic torque, only a single parameter from the machines is required by DTC which is the machine resistance value.

Despite the advantages, conventional DTC which utilises hysteresis controllers inherently operates with varying switching frequency. Not only that, a large torque ripple is also produced since conventional DTC fed by two-level inverter has limited selection of voltage vectors. A lot of research had been conducted to overcome these problem. One of the proposed solution which maintain the original structure of conventional DTC is by using a dithering technique [1]. Instead of directly fed flux and torque error into the hysteresis controllers, this technique injects a high frequency triangular waveform into the stator flux and

torque errors. Nevertheless, this method produces high switching frequency and consequently increases switching losses which is not suitable for high power applications. A switching strategy with minor modification on structure of conventional DTC drives to produce a constant switching frequency is proposed in [2]. Here, a three-level torque hysteresis controller is replaced with a new controller which consists of two triangular waveforms generators, a comparator and a PI controller. An extension of the proposed strategy towards the flux hysteresis controller is implemented in [3] in order to make improvement with the flux ripple. In both researches, a constant switching frequency is obtained since the inverter switching frequency is mainly affected by switching frequency in the torque hysteresis bandwidth [4].

Other proposed solution to improve the performance of conventional DTC drives is the implementation of Space Vector Modulation (SVM) scheme which is usually referred as DTC-SVM. There are various strategies for DTC-SVM approach which can classified as DTC-SVM (a) with PI controller [5]-[7] (b) with predictive or dead-beat controller [8] (c) fuzzy logic and/or neural networks [9] and (d) variable structure control (VSC) [10]-[12]. However, the adaptation of SVM increases the complexity of the DTC drive which somehow affecting the accuracy of control performance and the torque control dynamic performance. Multilevel inverters provide a higher number of voltage vectors than two-level inverters, hence offering more degree of freedom of vector selection. Lately, DTC drives fed by multilevel inverter such as Cascaded H-Bridge Multilevel Inverter (CHMI) [13],[14], Neutral Point Clamped (NPC) [15] and Flying Capacitor (FC) [16]-[17] as well as open-end winding configuration [18]-[19] have been considered for improvement of DTC performance.

This paper proposes a constant switching frequency torque controller for DTC of IM utilizing three-level NPC inverter with the purpose of produce a constant switching frequency and minimize torque ripple. The improvement obtained using the proposed method is verified via experimental results.

2. CONVENTIONAL DTC DRIVES

DTC drives was first introduced by I. Takahashi and T. Noguchi in 1986 [20]. This scheme attracts great attention by researcher as it offers less torque ripple, robust and simple structure as compared to FOC [21]. The structure of the conventional DTC of IM drives is illustrated in Figure 1. It consist of a pair of hysteresis controller, look-up table, voltage source inverter (VSI), voltage calculation, *d-q* current calculation, sector detection and estimator of flux and torque. Three-level hysteresis controller is used to control the torque while two-level hysteresis controller is used to control the flux. The output of both hysteresis controllers as well as the information of sector detection are fed to the look-up table (Table 1) in order to produce suitable switching states. The switching states becomes the input of VSI and the voltage calculation.

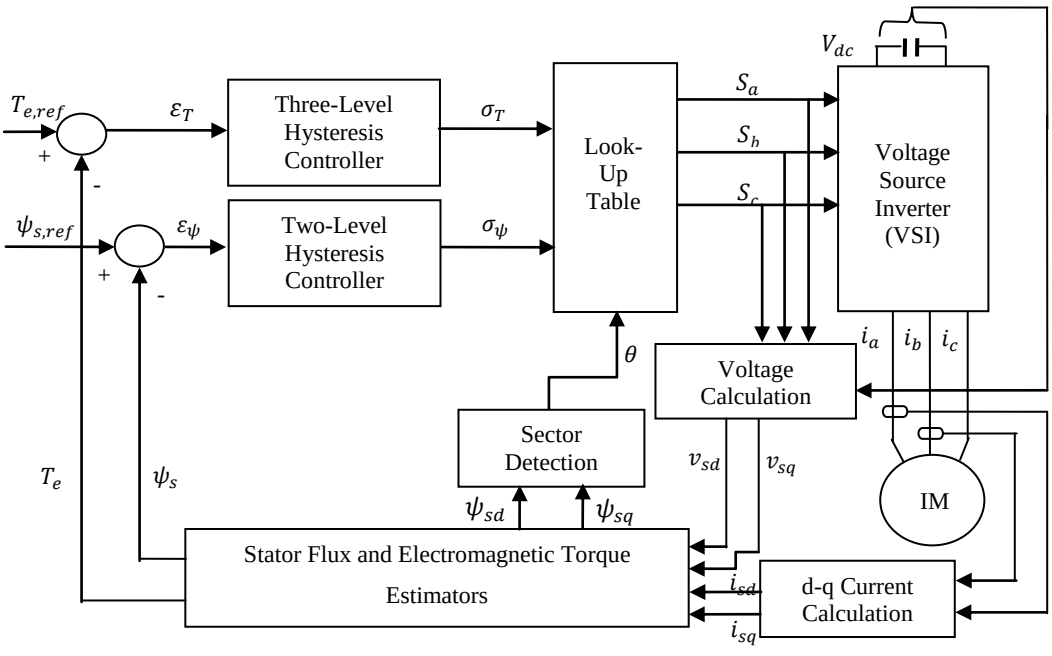

Figure 1. Structure of Conventional DTC of Induction Motor Drives

Table 1. Look-up table for selection of voltage vectors

Flux Error Status, σ_ψ	Torque Error Status, σ_T	Sector I	Sector II	Sector III	Sector IV	Sector V	Sector VI
1		$\bar{v}_{s2}$ [100]	$\bar{v}_{s3}$ [110]	$\bar{v}_{s4}$ [010]	$\bar{v}_{s5}$ [011]	$\bar{v}_{s6}$ [001]	$\bar{v}_{s1}$ [101]
	+3	$\bar{v}_{s0}$ [000]	$\bar{v}_{s7}$ [111]	$\bar{v}_{s0}$ [000]	$\bar{v}_{s7}$ [111]	$\bar{v}_{s0}$ [000]	$\bar{v}_{s7}$ [111]
	0	$\bar{v}_{s6}$ [001]	$\bar{v}_{s1}$ [101]	$\bar{v}_{s2}$ [100]	$\bar{v}_{s3}$ [110]	$\bar{v}_{s4}$ [010]	$\bar{v}_{s5}$ [011]
	-3	$\bar{v}_{s3}$ [110]	$\bar{v}_{s4}$ [010]	$\bar{v}_{s5}$ [011]	$\bar{v}_{s6}$ [001]	$\bar{v}_{s1}$ [101]	$\bar{v}_{s2}$ [100]
0	+3	$\bar{v}_{s7}$ [111]	$\bar{v}_{s0}$ [000]	$\bar{v}_{s7}$ [111]	$\bar{v}_{s0}$ [000]	$\bar{v}_{s7}$ [111]	$\bar{v}_{s0}$ [000]
	0	$\bar{v}_{s5}$ [011]	$\bar{v}_{s6}$ [001]	$\bar{v}_{s1}$ [101]	$\bar{v}_{s2}$ [100]	$\bar{v}_{s3}$ [110]	$\bar{v}_{s4}$ [010]
	-3						

Figure 2 shows the two-level three-phase voltage source inverter (VSI) circuit. It consists of a dc source V_{dc} and two IGBTs for each inverter leg/phase. The upper switches for every phase is represented by S_x, where x is phase a, b or c. Noted that, the switching state of the lower switches ($\overline{S_x}$) must be complementary with the upper switches. For example, if the upper switch of phase *a* is turned ON, (S_a = 1), the lower switch of phase *a* must be turned OFF ($\overline{S_a}$ = 0). The inverter produces eight switching states which consists of six active vectors ($\bar{v}_{s1} - \bar{v}_{s6}$) and two zero vectors ($\bar{v}_{s0}$ and $\bar{v}_{s7}$) which located at the origin of d-q axis as shown in Figure 3.

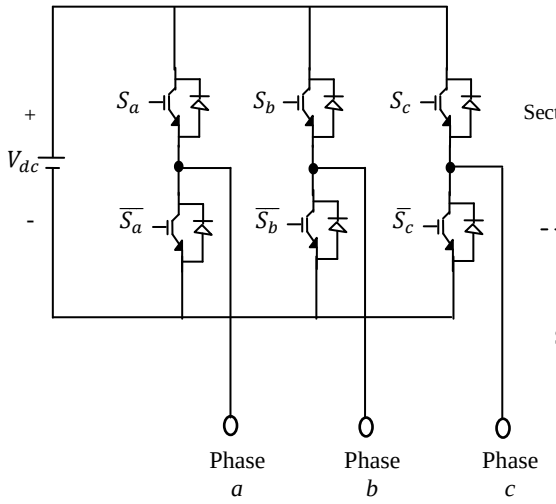

Figure 2. A three-phase VSI circuit

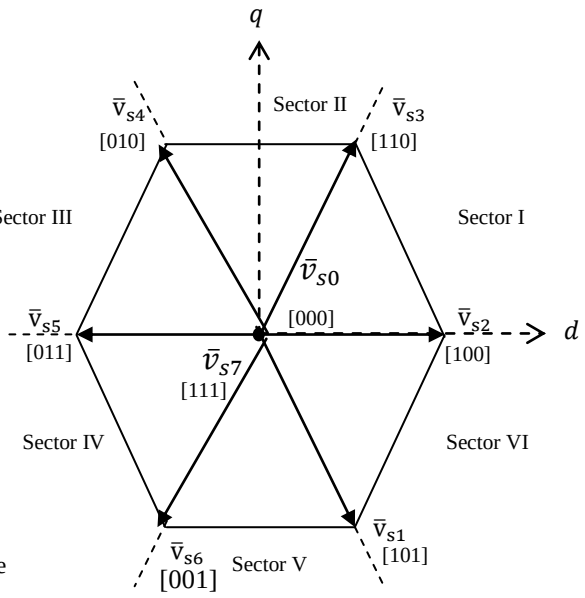

Figure 3. Voltage vectors of three-phase VSI

3. THREE-LEVEL NEUTRAL-POINT CLAMPED (NPC) INVERTER

Three-level NPC inverter was initially proposed by A. Nabae et. al in 1981 [22]. The structure of the inverter with connected to three-phase load (or IM) is shown in Figure 4. It consists of a dc source V_{dc}, two capacitors, six diodes and twelve switches (IGBTs). Terminal *P* and *N* represent the positive and negative terminals as they are connected to the positive and negative of V_{dc} respectively. Meanwhile, terminal *O* is defined as a point between two capacitors and it is also known as neutral point. Noted that, *n* is the neutral point of three-phase load (or IM).

Figure 5 illustrates the mapping of voltage vectors produced by the three-level NPC inverter. The voltage vectors form two hexagons (inner and outer) with the origin is defined as the point of reference. The inverter comprises of 27 switching states but only 19 voltage vectors are available since six voltage vectors in inner hexagon have a redundant switching state. These voltage vectors can be categorized into four types

based on their amplitude which are long, medium, short and zero voltage vectors. Table 3 shows the type, switching state and magnitude of each type of voltage vectors.

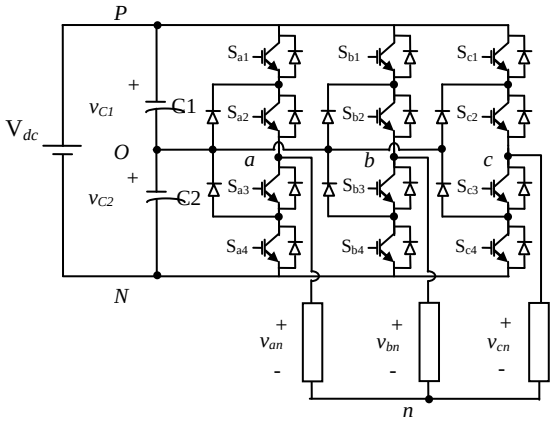

Figure 4. A three-level NPC inverter

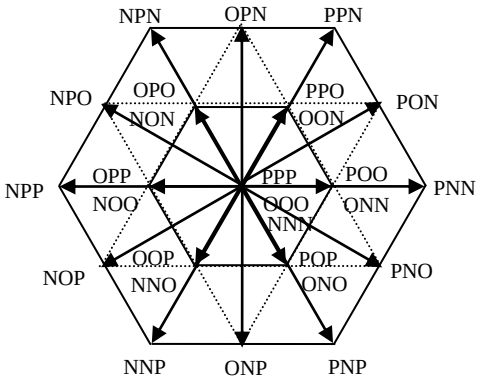

Figure 5. Voltage vectors produced by three-level NPC inverter

Table 3. Type of voltage vectors and magnitude of three-level NPC

Type of voltage vector	Switching State	Magnitude
Long amplitude	PPN, PNN, PNP, NNP, NPP, NPN	$2V_d / 3$
Medium amplitude	OPN, PON, PNO, ONP, NOP, NPO	$V_d / \sqrt{3}$
Short amplitude	PPO, POO, POP, OOP, OPP, OPO, OON, ONN, ONO, NNO, NOO, NON	$V_d / 3$
Zero amplitude	PPP, OOO, NNN	0

4. CONSTANT SWITCHING FREQUENCY (CSF) TORQUE CONTROLER FOR DTC OF IM DRIVES WITH TWO-LEVEL INVERTER

One of the proposed solution to produce a constant switching frequency and minimize torque ripple of conventional DTC drives with two-level inverter is by replacing the torque hysteresis controller with a Constant Switching Frequency (CSF) torque controller [23]-[25]. Figure 6 shows a block diagram of the CSF torque controller which consists of two triangular carrier waveforms, C_{upper} and C_{lower} that are 180° out of phase to each other, two comparators and a PI controller. Structure of the PI controller is illustrated in Figure 7. The compared output between $T_{e,ref}$ and T_e are fed to the PI controller which consist of $K_p$and K_i gain and also discrete-time integrator blocks. The output from the PI controller, T_{pi} is then compared with C_{upper} and C_{lower} to produce the torque error status (S_T). S_T has three different status; 1, 0 and -1; which are similar to status produce by hysteresis controller in order to maintain the simplicity of the conventional DTC. However, using the CSF technique, the status of S_T is governed as follows:

$$S_T = \begin{cases} 1 & \text{for } \mathrm{T_{pi}} \geq \mathrm{C_{upper}} \\ 0 & \text{for } \mathrm{C_{lower}} < \mathrm{T_{pi}} < \mathrm{C_{upper}} \\ -1 & \text{for } \mathrm{T_{pi}} \leq \mathrm{C_{lower}} \end{cases} \quad (1)$$

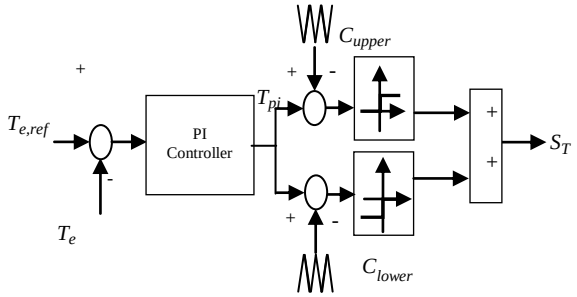

Figure 6. Block diagram of CSF torque controller for two-level DTC drives

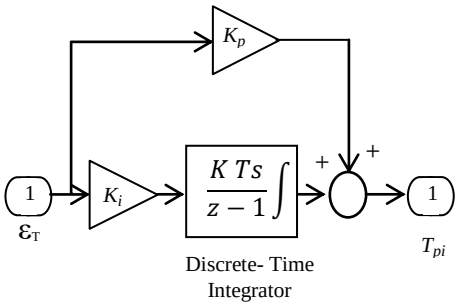

Figure 7. Structure of PI Controller

The modelling of torque loop is required in order to determine the parameters the the PI controller [19]. First, the modelling of IM in stationary reference frame can be given as follows:

$$\bar{v}_s = R_s\bar{i}_s + \frac{d\bar{\psi}_s}{dt} \tag{2}$$

$$0 = R_r\bar{i}_r + \frac{d\bar{\psi}_r}{dt} - j\omega_r\bar{\psi}_r \tag{3}$$

$$\bar{\psi}_s = L_s\bar{i}_s + L_m\bar{i}_r \tag{4}$$

$$\bar{\psi}_r = L_r\bar{i}_r + L_m\bar{i}_s \tag{5}$$

$$T_e = \frac{3}{2}P\,\bar{\psi}_s \times \bar{i}_s \tag{6}$$

where $\bar{\psi}_s$ and $\bar{\psi}_r$ are stator and rotor fluxes, $\bar{v}_s$ is stator voltage, ω_r represents rotor speed, L_s, L_r and L_m denote stator, rotor and mutual inductances, $\bar{i}_s$ and $\bar{i}_r$ are stator and rotor currents, T_e is electromagnetic torque while P is number of pole pair. By using (2)-(6), the positive and negative slope of torque equations ($\frac{dT_e^+}{dt}$ and $\frac{dT_e^-}{dt}$) could be obtained as below [26],[27]:

$$\frac{dT_e^+}{dt} = -T_e\left(\frac{1}{\sigma\tau_s} + \frac{1}{\sigma\tau_r}\right) + \frac{3}{2}P\frac{L_m}{\sigma L_s L_r}\left[(\bar{v}_s - j\omega_r\bar{\psi}_s) \bullet j\bar{\psi}_r\right] \tag{7}$$

$$\frac{dT_e^-}{dt} = -T_{e,c}\left(\frac{1}{\sigma\tau_s} + \frac{1}{\sigma\tau_r}\right) - \frac{3}{2}P\frac{L_m}{\sigma L_s L_r}\left[(j\omega_r\bar{\psi}_s) \bullet j\bar{\psi}_r\right] \tag{8}$$

where σ is leakage coefficient. Equations (7) and (8) are then simplified and written in stationary reference frame in terms of synchronous speed and duty ratio as follows:

$$\frac{dT_e^+}{dt} = -AT_e + B\bar{v}_s + K\left(\frac{\omega_s}{d} - \omega_r\right) \tag{9}$$

$$\frac{dT_e^-}{dt} = -AT_e - K\omega_r \tag{10}$$

where,

$$A_t = \frac{1}{\sigma\tau_{sr}} \tag{11}$$

$$B_t = \frac{3pL_m\varphi_s}{4\sigma L_s L_r} \tag{12}$$

$$K_t = \frac{3pL_m\varphi_s\varphi_r^{\varphi_s}}{4\sigma L_s L_r} \tag{13}$$

Figure 8 shows the block diagram of linearized torque equation which it is determined by using (9). The torque Equation, expressed in frequency domain is given as (14).

$$T_e(s) = \frac{B\bar{v}_s d(s) + K\omega_{slip}(s)}{s+A} \quad (14)$$

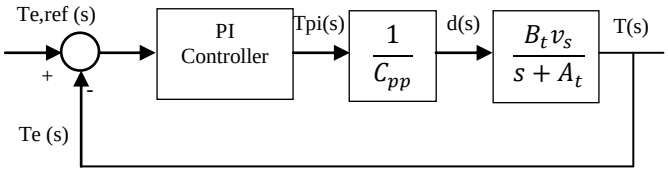

Figure 8. Linearized torque loop block diagram

5. PROPOSED CSF TORQUE CONTROLLER FOR DTC OF IM DRIVES WITH THREE-LEVEL NPC INVERTER

For the DTC of IM drives with three-level NPC inverter, the proposed CSF torque controller consists of a PI controller, six hysteresis comparators and six triangular waveforms (Carrier 1, 2, 3, 4, 5 and 6) as illustrated in Figure 9. Carrier 1, 2 and 3 are 180° out of phase with Carrier 4, 5, and 6. The structure of the PI controller is similar as in two-level DTC drives shown in Figure 7. As can be noticed, hysteresis comparator is also included in the proposed controller. However, unlike the conventional DTC drives, the comparator is used for comparison of output of PI controller and triangular carrier waveform. The torque controller produces status S_T which are similar with seven-level hysteresis controller [28]. The status of the proposed torque controller is obtained as follows:

$$S_T = \begin{cases} 3, & \text{for Tpi} \geq \text{Carrier 1} \\ 2, & \text{for Carrier 2} \leq \text{Tpi} < \text{Carrier 1} \\ 1, & \text{for Carrier 3} \leq \text{Tpi} < \text{Carrier 2} \\ 0 & \text{for Carrier 4} \leq \text{Tpi} < \text{Carrier 3} \\ -1, & \text{for Carrier 5} \leq \text{Tpi} < \text{Carrier 4} \\ -2, & \text{for Carrier 6} \leq \text{Tpi} < \text{Carrier5} \\ -3, & \text{for Tpi} < \text{Carrier 6} \end{cases}$$

Figure 10 illustrates the triangular carrier waveforms for the proposed controller which consist of three sets of isosceles triangles. Carrier 3 is utilized for low speed operation, Carrier 2 is for medium speed operation and Carrier 1 signifies the high speed operation. By referring to the figure, absolute slope of Carrier 3 (i.e. low speed operation) and Carrier 1 (i.e. high speed operation) can be calculated using Equation (15) and (16):

$$Absolute\ Slope\ of\ Carrier\ 3 = \frac{\Delta y_L}{\Delta t_L} = \frac{C_{pp,L}}{T_{tri,L}/_2} = 2f_{tri,L}C_{pp,L} \quad (15)$$

$$Absolute\ Slope\ of\ Carrier\ 1 = \frac{\Delta y_H}{\Delta t_H} = \frac{C_{pp,H}}{T_{tri,H}/_2} = 2f_{tri,H}C_{pp,H} \quad (16)$$

where $T_{tri,L}$ is the period of Carrier 3 (or $T_{tri,H}$ is the period of Carrier 1) of proposed controller, $f_{tri,L}$ denotes the frequency of Carrier 3 (or $f_{tri,H}$ denotes the frequency of Carrier 1) for low speed operation and $C_{pp,L}$ (or $C_{pp,H}$) indicates the peak to peak magnitude of Carrier 3 (or Carrier 1). Equation (15) is valid to determine the absolute slope of Carrier 2 (i.e. medium speed operation). This is because the magnitude and period of the Carrier 2 are similar with Carrier 3.

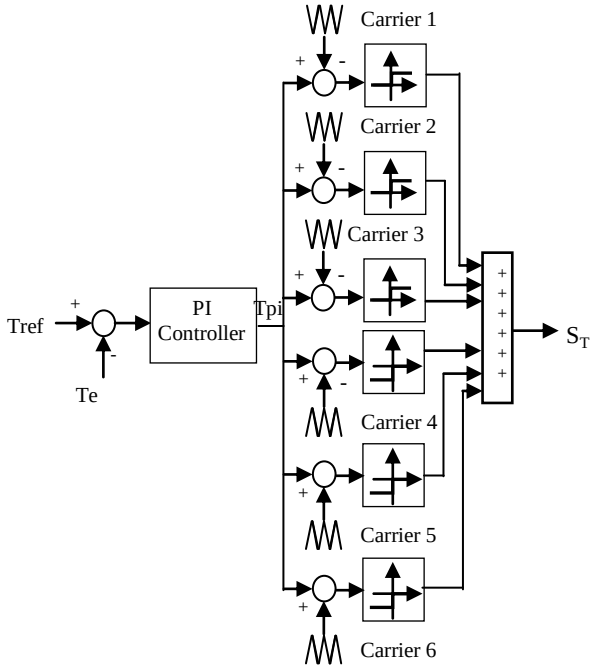

Figure 9. Proposed CSF torque controller for DTC of IM drives utilizing three-level NPC inverter

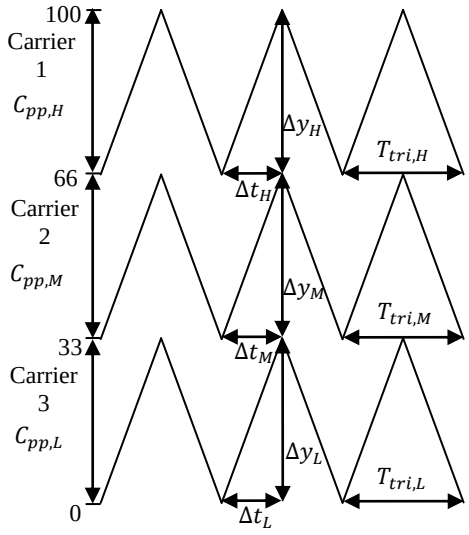

Figure 10. The triangular carrier waveform for proposed CSF torque controller

In general, the transfer function of the PI controller is written as follows:

$$\frac{T_{PI}(s)}{\varepsilon_T(s)} = K_p + \frac{K_i}{s} \tag{17}$$

where K_p is proportional gain and K_i is integral gain. The PI controller has to be designed based on the constraint that the slope of T_{pi} must not exceed the absolute of triangular carrier waveform. Noted that, the slope of T_{pi} is influenced by K_p. For low, medium and high speed operation, the PI controller are designed as follow:

5.1. Case 1: Low Speed Operation

The Equation of positive slope of torque at low speed operation are rewritten from (9):

$$\frac{dT_e^+}{dt} = -AT_e + B\bar{v}_{s,S} + K\left(\frac{\omega_s}{d_L} - \omega_r\right) \tag{18}$$

Based on above equations, design of PI controller for positive slope must satisfied the Equation (18).

$$Absolute\ Slope\ of\ Carrier\ 3 \geq \left[-AT_e + B\bar{v}_{s,S} + K\left(\frac{\omega_s}{d_L} - \omega_r\right)\right] K_{pL}^+ \tag{19}$$

The maximum positive slope is assumed to occur at zero rotor speed and at rated slip which are as follow:

$$\omega_r = 0$$
$$\omega_s = \omega_{slip} \tag{20}$$

The proposed DTC drives apply short amplitude of voltage vectors for increasing the torque. Hence, the magnitude of stator voltage of short amplitude of voltage vector, $\bar{v}_{s,S} = V_{dc}/3$. The term d_L in Equation (19) is expressed in (21) which it is represented for low speed condition.

$$d_L = \frac{AT_e - K\omega_{slip}}{B\bar{v}_{s,S}} \tag{21}$$

Therefore, by substituting (15), (20) and (21) into (19), the proportional gain for positive slope at low speed operation, (K_{pL}^{+}) can be written as follow:

$$K_{pL}^{+} \leq \frac{|2f_{tri,L}C_{pp,L}|}{\left|-AT_e + B\bar{v}_{s,S} + K\left(\frac{\omega_{slip}}{d_L} - \omega_r\right)\right|} \quad (22)$$

In contrast, the negative slope of torque equation in (10) is rewrite as follow:

$$\frac{dT_e^{-}}{dt} = -AT_e - K\omega_r \quad (23)$$

Equation (24) must be satisfied to determine the gain of proportional for negative slope of torque at low speed operation (K_{pL}^{-}).

$$Absolute\ Slope\ of\ Carrier\ 3 \geq [-AT_e - K\omega_r]K_{pL}^{-} \quad (24)$$

The maximum negative slope is assumed to occur at maximum speed achieved for low amplitude voltage vector (i.e. $\bar{v}_{s,S} = V_{dc}/3$). So, maximum ω_s reached at low speed is half of the ω_s in three-level NPC and it yield as follow:

$$\omega_s = \frac{\omega_{s,rated} v_{line}}{v_{line,rated}} \left(\frac{2\pi}{60} / 2\right) = \frac{\omega_{s,rated} v_{line}}{v_{line,rated}} \left(\frac{\pi}{60}\right) \quad (25)$$

$$\omega_r = \omega_s - \omega_{slip} \quad (26)$$

The zero amplitude voltage vectors (i.e. $\sigma_{TPC} = 0$) is employed for decreasing the torque at low speed operation of DTC drives. Thus, the magnitude of stator voltage of zero amplitude voltage vector, $\bar{v}_{s,Z} = 0$. Then, K_{pL}^{-} is obtained in Equation (27) by substituting (15), (25) and (26) into (24) and yield:

$$K_{pL}^{-} \leq \frac{|2f_{tri,L}C_{pp,L}|}{|-AT_e - K\omega_r|} \quad (27)$$

Thus, the smaller value between K_{pL}^{+} and K_{pL}^{-} is chosen as gain of proportional at low speed (K_{pL}) to make sure that the slope of T_{PI} will not exceed the slope of Carrier 3. The integral gain is determined as follows:

$$K_{iL} = K_{pL}A \quad (28)$$

5.2. Case 2: Medium Speed Operation

At medium speed operation, the positive slope of torque is given in (18). By taking into account (18), the condition in (29) must be satisfied so that the value of proportional gain of positive slope at medium speed (K_{pM}^{+}) can be obtained.

$$Absolute\ Slope\ of\ Carrier\ 2 \geq \left[-AT_e + B\bar{v}_{s,M} + K\left(\frac{\omega_s}{d_M} - \omega_r\right)\right] K_{pM}^{+} \quad (29)$$

It is assumed that the maximum positive slope is occurred at the maximum speed achieved for short amplitude of voltage vectors (i.e. $\bar{v}_{s,S} = V_{dc}/3$). Equation (30) and (31) are written for ω_r and ω_s.

$$\omega_r = \omega_s - \omega_{slip} \quad (30)$$

$$\omega_s = \omega_r + \omega_{slip} \quad (31)$$

The medium amplitude voltage vectors is employed in proposed method to increase the torque and the magnitude $\bar{v}_{s,M} = V_{dc}/\sqrt{3}$. The term d_M in (29) denotes continuous duty ratio of medium speed operation.

$$d_M = \frac{AT_e - K\omega_{slip}}{B\bar{v}_{s,M}} \quad (32)$$

By substituting (15), (30), (31) and (32) into (29), K_{pM}^{+} are expressed as follows:

$$K_{pM}^{+} \leq \frac{|2f_{tri,M}C_{pp,M}|}{\left|-AT_e+B\bar{v}_{s,M}+K\left(\frac{\omega_S}{d_M}-\omega_r\right)\right|} \quad (33)$$

On the other hand, the Equation of negative slope of torque is presented in (34). As can be noticed, the positive and negative slope are using same equation. This is due to the application of voltage vector for decreasing the torque in negative slope is no longer zero amplitude voltage vectors as applied at low speed operation.

$$\frac{dT_e^{-}}{dt} = -AT_e + B\bar{v}_{s,M} + K\left(\frac{\omega_s}{d_L} - \omega_r\right) \quad (34)$$

The design of PI controller must meet the condition as follows:

$$Absolute\ Slope\ of\ Carrier\ 2 \geq \left[-AT_e + B\bar{v}_{s,S} + K\left(\frac{\omega_s}{d_M} - \omega_r\right)\right] K_{pM}^{-} \quad (35)$$

The maximum negative slope is assumed to occur at maximum speed achieved for medium amplitude of voltage vector (i.e. $\bar{v}_{s,M} = V_{dc}/\sqrt{3}$). So, ω_r is determined from (30) and the maximum ω_s is obtained by using (36).

$$\omega_s = \frac{\omega_{s,rated}v_{line}}{v_{line,rated}} \left(\frac{2\pi}{60}\right)\left(\frac{\sqrt{3}}{2}\right) \quad (36)$$

The short amplitude of voltage vectors is chosen for decreasing the torque at medium speed operation of the proposed method. Then, by substituting (15), (30), (36) into (37).

$$K_{pM}^{-} \leq \frac{|2f_{tri,M}C_{pp,M}|}{\left|-AT_e+B\bar{v}_{s,S}+K\left(\frac{\omega_S}{d_M}-\omega_r\right)\right|} \quad (37)$$

Therefore, the smaller value of K_{pM}^{+} and K_{pM}^{-} is selected as K_{pM} to ensure that the slope of T_{PI} not exceed the slope of Carrier 2. The integral gain is obtained as follows:

$$K_{iM} = K_{pM}A \quad (38)$$

5.3. Case 3: High Speed Operation

For this operation, the positive slope of torque is given in (18) and based on it, the proportional gain of positive slope at high speed operation (K_{pH}^{+}) can be determined and the condition in (39) must be satisfied.

$$Absolute\ Slope\ of\ Carrier\ 1 \geq \left[-AT_e + B\bar{v}_{s,L} + K\left(\frac{\omega_s}{d_H} - \omega_r\right)\right] K_{pH}^{+} \quad (39)$$

The maximum positive slope is assumed to occur at maximum speed achieved for medium amplitude of voltage vectors (i.e. $\bar{v}_{s,M} = V_{dc}/\sqrt{3}$). Long amplitude of voltage vectors is employed in proposed method to increase the torque and the magnitude, $\bar{v}_{s,L} = 2V_{dc}/3$. The continuous duty ratio of high speed operation is represented by d_H is written in (40).

$$d_H = \frac{AT_e - K\omega_{slip}}{B\bar{v}_{s,L}} \quad (40)$$

Thus, by substituting (16), (30), (31) and (40) into (39), K_{pH}^{+} are obtained as follow:

$$K_{pH}^{+} \leq \frac{|2f_{tri,H}C_{pp,H}|}{\left|-AT_e+B\bar{v}_{s,L}+K\left(\frac{\omega_S}{d_H}-\omega_r\right)\right|} \quad (41)$$

Conversely, the negative slope of torque is written in (34). Noted that the equation of negative slope is similar with medium speed operation which the selection of voltage vectors is differ from low speed condition.

$$Absolute\ Slope\ of\ Carrier\ 1 \geq \left[-AT_e + B\bar{v}_{s,S} + K\left(\frac{\omega_s}{d_H} - \omega_r\right)\right] K_{pH}^{-} \quad (42)$$

The maximum negative slope is assumed to occur at maximum speed achieved for long amplitude of voltage vector (i.e. $\bar{v}_{s,L} = 2V_{dc}/3$). So, ω_r is determined by using (30) and the maximum ω_s is expressed in (43).

$$\omega_s = \frac{\omega_{s,rated} v_{line}}{v_{line,rated}} \left(\frac{2\pi}{60}\right) \quad (43)$$

The short amplitude of voltage vectors is chosen for decreasing the torque at high speed operation of the DTC drives. Then, the proportional gain for negative slope at high speed operation (K_{pH}^{-}) is given in Equation (44) by substituting (16), (30), (32) and (43) into (41).

$$K_{pH}^{-} \leq \frac{|2 f_{tri,H} C_{pp,H}|}{\left|-AT_e + B\bar{v}_{s,S} + K\left(\frac{\omega_S}{d_M}\omega_r\right)\right|} \quad (44)$$

Therefore, the smaller value of K_{pH}^{+} and K_{pH}^{-} is selected as gain of proportional at high speed operation (K_{pH}) to ensure that the slope of T_{PI} not exceed the slope of Carrier 1. The integral gain is obtained as written in (44).

$$K_{iH} = K_{pH} A \quad (45)$$

For this research, the value (or gain) of the PI controller parameters of the proposed CSF torque controller for low, medium and high speed operation are given in Table 4.

Table 4. Parameters of proposed CSF torque controller for low, medium and high speed operation

Parameter	Value
K_{pl}	188.43
K_{il}	382.67
K_{pm}	51.81
K_{im}	19828.0
K_{ph}	28.96
K_{ih}	11083.0

Figure 11 shows the complete structure of DTC of IM drives using three-level NPC inverter with the proposed torque controller. As can be seen, the original structure and simplicity of conventional DTC drive are still being maintained as the torque controller is only used to replace the hysteresis-based controller of conventional DTC drives. NPC inverter have major problem which is imbalance of upper and lower capacitor. Hence, the Balancing Control Strategy block is applied to overcome the problem. This block requires the information of upper and lower capacitor voltage.

6. EXPERIMENTAL SETUP AND RESULTS

The workability of the proposed method had been carried out using experimental setup shown in Figure 12. The setup consists of DSPACE 1104 controller board, Field Programmer Gate Array (FPGA), NPC inverter, gate drivers, voltage sensor, current sensor, IM and DC generator. The proposed method is implemented on DSPACE 1104 board. The experiment was performed by using IM and DC generator acts as loading unit. The parameters of the induction motor used in the experiment are given in Table 5.

The experimental results by using two approaches which are DTC of IM with NPC inverter using hysteresis controller (with acronym of DTC-NPC-HTC) and DTC of IM with NPC inverter using proposed CSF controller (with acronym of DTC-NPC-CSF) are provided in order to analyze the improvement of DTC drives in terms of torque ripple and switching frequency. The experimental works are performed for three different operations which are low, medium and high speed.

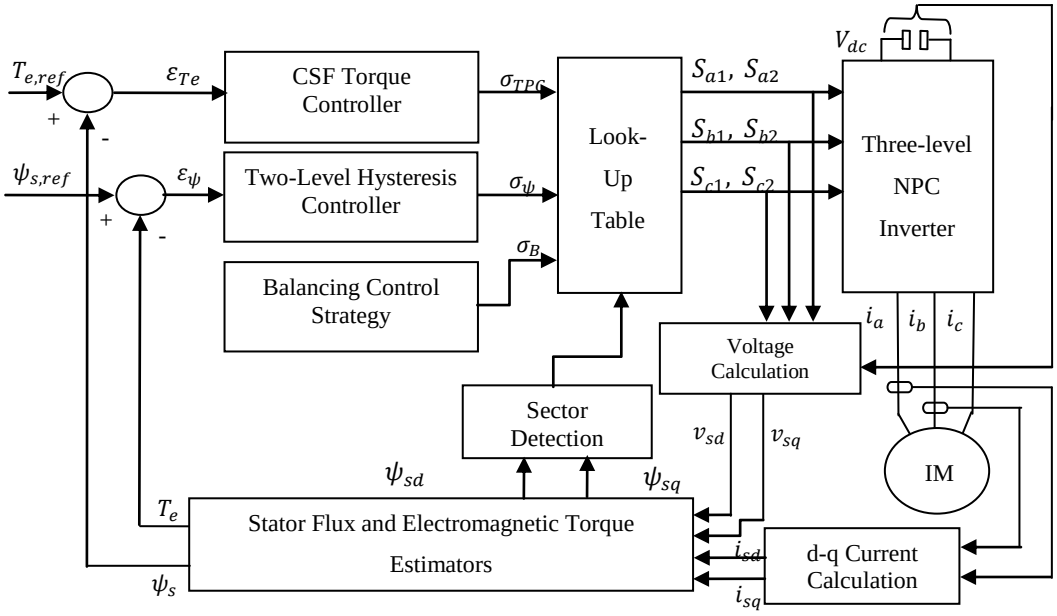

Figure 11. . Proposed Control Structure of DTC of Induction Motor Drives Utilizing Three-Level NPC Multilevel Inverter

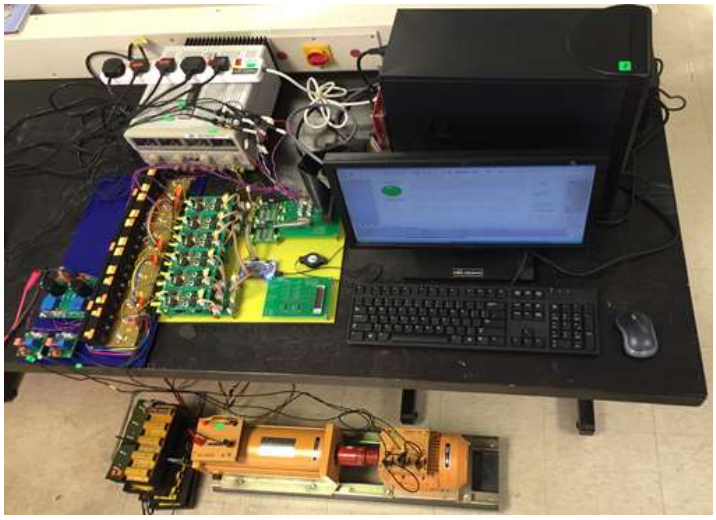

Figure 12. Experimental platform for DTC of induction motor drives using three-level NPC inverter with CSF torque controller the proposed method

Table 5. The parameter of induction motor

Parameter	Value
Stator resistance, R_s	6.1 Ω
Rotor resistance, R_r	6.2298 Ω
Stator self-inductance, L_s	0.47979 mH
Rotor self-inductance, L_r	0.47979 mH
Mutual inductance, L_m	0.4634 mH
Number of poles, *P*	2
Stator flux rated, $\psi_{s,rated}$	0.8452 Wb
Torque rated, $T_{e,rated}$	1.3 Nm
DC Voltage, V_{dc}	180 V
Sampling period	50 µs

The frequency spectrum of DTC-NPC-HTC and DTC-NPC-CSF approaches are presented in Figure 13. Based on the figure, it can be observed that the switching frequency of DTC-NPC-HTC varies with the motor speed. For low speed operation, the dominant switching harmonic is 1.25 kHz. However, for medium and high speed operation, the harmonics are scattered below 1.25 kHz. The concentration of the harmonics varies with motor speed operation and is unpredictable for different speed condition. On the other hand, DTC-NPC-CSF operates at constant switching frequency regardless of the speed as the dominant switching frequency is always mapped at 2.5 kHz (which is the frequency of triangular carrier waveform).

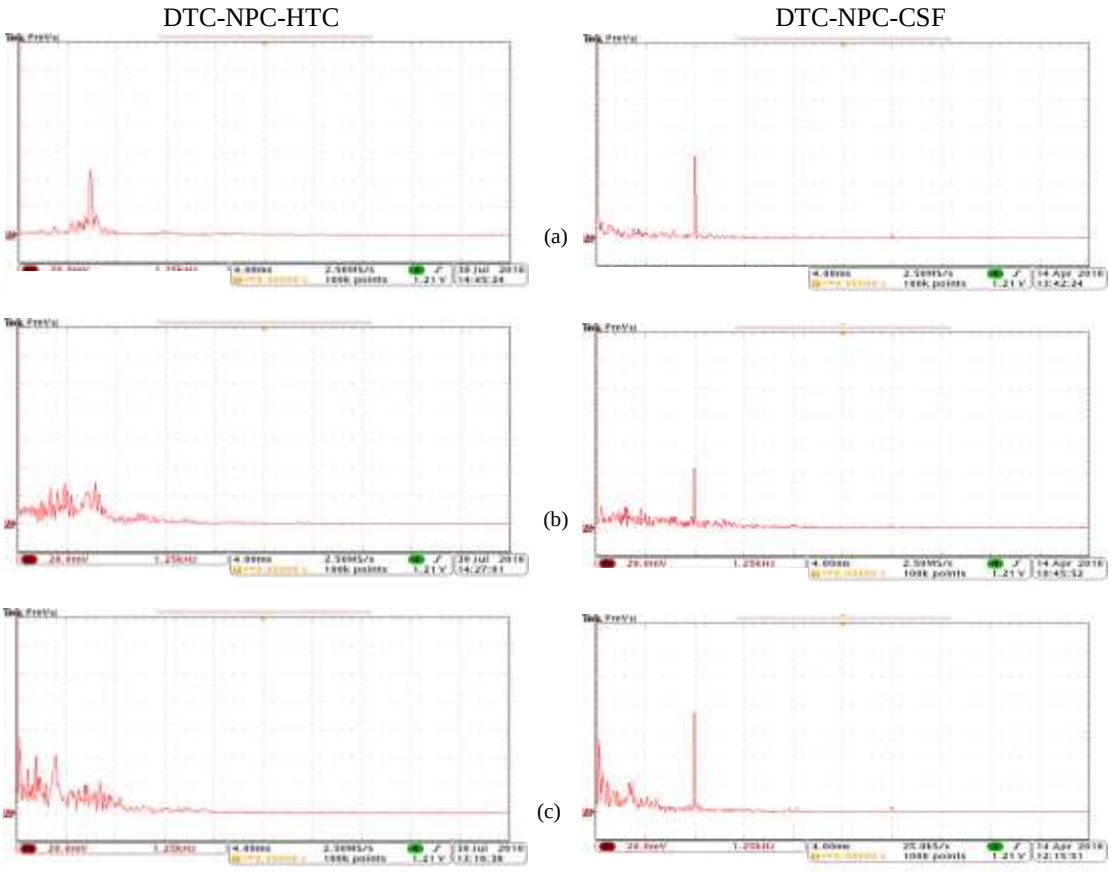

Figure 13. Frequency spectrum of torque for DTC-NPC-HTC (left) and DTC-NPC-CSF (right) for (a) low (b) medium and (c) high speed operation

Figure 14 depicts the torque waveforms of DTC-NPC-HTC and DTC-NPC-CSF for low, medium and high speed operation. The results of DTC-NPC-HTC consists of torque reference ($T_{e,ref}$), actual torque (T_e) and torque error (T_{err}) while output of PI controller (T_{pi}), three triangular carrier waveforms (Carrier 1, 2 and 3) as well as $T_{e,ref}$, T_e, are presented for DTC-NPC-CSF. Noted that, the triangular carrier waveforms regulates the torques at different speed operations as T_{pi} is being compared with carrier 1, 2 and 3 for operation at high, medium and low speed respectively.For the DTC-NPC-HTC, the torque and flux references are set at 1.3 Nm and 0.8452 Wb which it also is their rated values while their hysteresis bandwidths are set at 15.0 % and 1.0 % of their rated values. As for DTC-NPC-CSF, the frequency of triangular carrier is set at 2.5 kHz and their magnitude are spreads equally between 0 and 100 units. Moreover, the voltage vector for DTC-NPC-CSF are selected of based on the operating conditions. Short and zero amplitude voltage vectors are applied for low speed operation while medium and short amplitude voltage vectors are employed for medium speed operation. For high speed operation, long and short amplitude voltage vectors are required [15].

From Figure 14, T_e of both approaches regulate steadily at $T_{e,ref}$. However, in terms of torque ripple, DTC-NPC-CSF produces lower torque ripple than DTC-NPC-HTC. As can been noticed, T_{pi} is well

regulated at Carrier 3 for low speed operation, while for medium and high speed, T_{pi} are regulated at Carrier 2 and 1 respectively. As can be seen also, the slope of T_{pi} has also been ensured to not exceed the slope of the carrier, based on the appropriate selection of K_p and K_i of PI controller. Otherwise, overshoot as well as undershoot occurs and the torque ripple is not minimized.

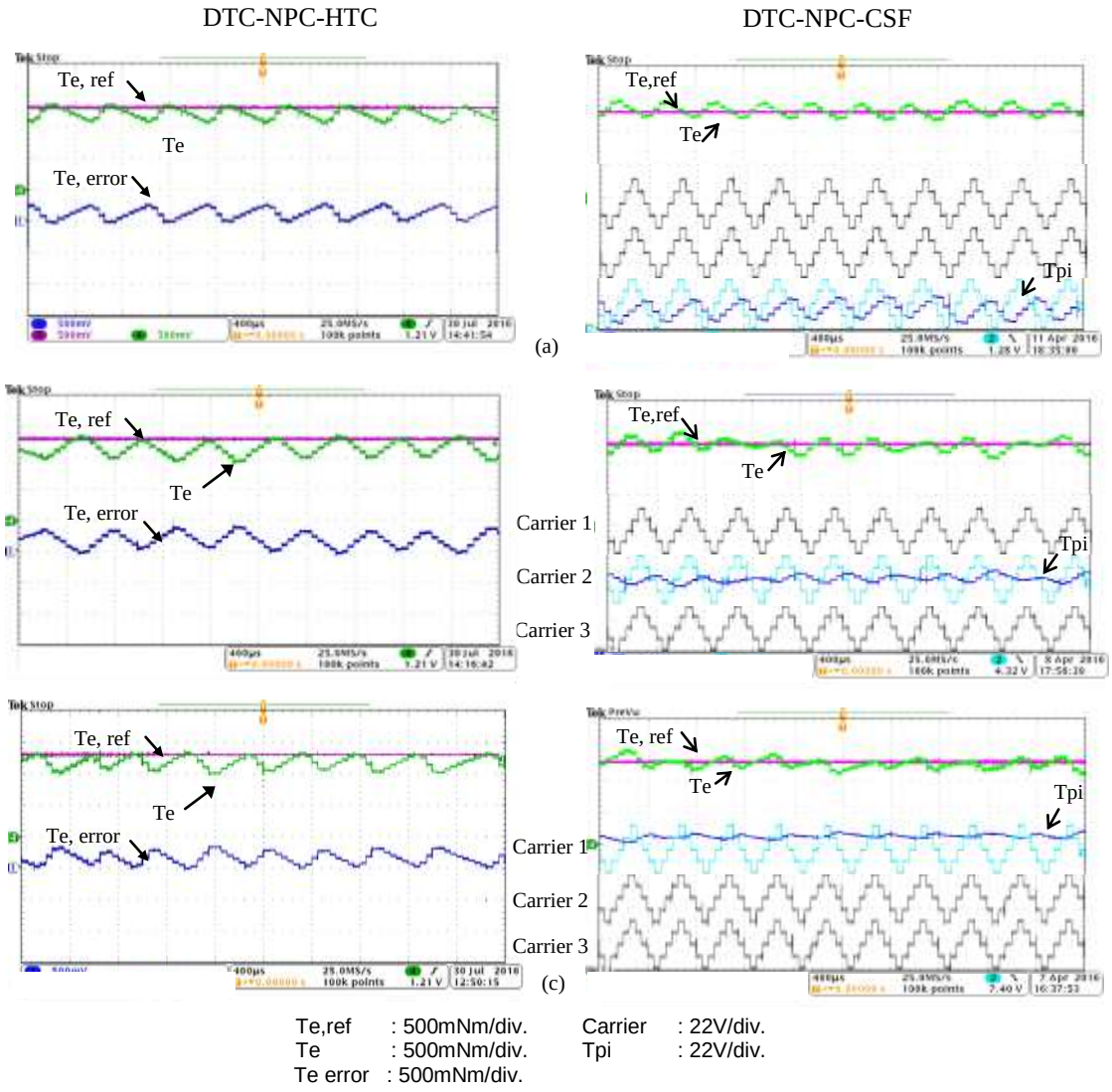

Figure 14. Torque waveform of DTC-NPC-HTC (left) and DTC-NPC-CSF (right) for (a) low (b) medium and (c) high speed operation

7. CONCLUSION

This paper introduces a constant switching frequency torque controller for DTC of induction motor drives utilizing three-level NPC inverter. The proposed controller which consist of PI controller is used to replace torque hysteresis controller in order to produce a constant switching frequency and minimise torque ripple. These improvement are obtained by appropriately determine the value of controller gains (K_p and K_i) so that the slope of output from the PI controller does not exceed the slope of carrier waveform. The value of the controller gains are determined using mathematical equations for three different speed operation (i.e. low, medium and high speed). The performance of the NPC fed DTC of induction motor drives with the proposed torque controller are validated through experimental results.

ACKNOWLEDGEMENTS

The authors would like to thank the Ministry of Education (MOE) Malaysia and Universiti Teknikal Malaysia Melaka (UTeM) for providing the research grant FRGS/1/2015/TK04/FTK/03/F00285 to conduct this research.

REFERENCES

[1] T. Noguchi, *et al.*, "Enlarging switching frequency in direct torque-controlled inverter by means of dithering," *IEEE Transactions on Industry Applications*, vol. 35, pp. 1358-1366, 1999.
[2] N. R. N. Idris and A. H. M. Yatim, "Reduced torque ripple and constant torque switching frequency strategy for direct torque control of induction machine," in *Applied Power Electronics Conference and Exposition, 2000. APEC 2000. Fifteenth Annual IEEE*, vol. 1, pp. 154-161, 2000.
[3] C. L. Toh, *et al.*, "New torque and flux controllers for direct torque control of induction machines," in *Power Electronics and Drive Systems, 2003. The Fifth International Conference on*, vol. 1, pp. 216-221, 2003.
[4] D. Casadei, *et al.*, "Effect of flux and torque hysteresis band amplitude in direct torque control of induction motor," *Conf. Rec., IEEE IECON 1994*, pp. 299-304, 1994.
[5] Y. Xue, *et al.*, "A low cost stator flux oriented voltage source variable speed drive," in *Conference Record of the 1990 IEEE Industry Applications Society Annual Meeting*, vol. 1, pp. 410-415, 1990.
[6] M. Zelechowski, "Space Vector Modulated – Direct Torque Controlled (DTC – SVM) Inverter – Fed Induction Motor Drive," Faculty of Electrical Engineering, Warsaw University of Technology, Poland, 2005.
[7] A. Tripathi, *et al.*, "Dynamic control of torque in overmodulation and in the field weakening region," *IEEE Transactions on Power Electronics*, vol. 21, pp. 1091-1098, 2006.
[8] L. J. Hui, *et al.*, "A dead-beat type digital controller for the direct torque control of an induction motor," *IEEE Transactions on Power Electronics*, vol. 17, pp. 739-746, 2002.
[9] P. Z. Grabowski, *et al.*, "A simple direct-torque neuro-fuzzy control of PWM-inverter-fed induction motor drive," *IEEE Transactions on Industrial Electronics*, vol. 47, pp. 863-870, 2000.
[10] C. Lascu and A. M. Trzynadlowski, "Combining the principles of sliding mode, direct torque control, and space-vector modulation in a high-performance sensorless AC drive," *IEEE Transactions on Industry Applications*, vol. 40, pp. 170-177, 2004.
[11] C. Lascu, *et al.*, "Variable-structure direct torque control - a class of fast and robust controllers for induction machine drives," *IEEE Transactions on Industrial Electronics*, vol. 51, pp. 785-792, 2004.
[12] Y. Zhang, *et al.*, "Sensorless sliding-mode control of induction motors," *IEEE Transactions on Industrial Electronics*, vol. 47, pp. 1286-1297, 2000.
[13] M. Z. R. Z. Ahmadi, *et al.*, "Improved Torque Control Performance in Direct Torque Control using Optimal Switching Vectors," *International Journal of Power Electronics and Drive System*, vol. 5, pp. 441-452, 2015.
[14] S. Ramahlingam, *et al.*, "Improved torque control performances using Torque Error Modulator for Multilevel Inverter based DTC induction motors," *Energy Conversion (CENCON), IEEE Conference on*, pp. 1-6, 2015.
[15] H. Ismail, *et al.*, "Direct Torque Control of induction machine using 3-level neutral point clamped inverter," *Research and Development (SCOReD), 2015 IEEE Student Conference on*, pp. 571-576, 2015.
[16] S. Du, *et al.*, "A Startup Method for Flying-Capacitor Modular Multilevel Converter (FC-MMC) with Effective Damping of LC Oscillations," *IEEE Transactions on Power Electronics*, pp. 1-1, 2016.
[17] M. F. Escalante, *et al.*, "Flying capacitor multilevel inverters and DTC motor drive applications," *IEEE Transactions on Industrial Electronics*, vol. 49, pp. 809-815, 2002.
[18] K. Rahim, *et al.*, "A dual mode DTC of open-end winding induction motor drive with reduced torque ripple," *Energy Conversion (CENCON), IEEE Conference on*, pp. 106-111, 2014.
[19] M. K. Rahim, *et al.*, "Reduced torque ripple and switching frequency using optimal DTC switching strategy for open-end winding of induction machines," *Power Electronics and Drive Systems (PEDS), IEEE International Conference on*, pp. 767-772, 2015.
[20] I. Takahashi and T. Noguchi, "A New Quick-Response and High-Efficiency Control Strategy of an Induction Motor," *Industry Applications, IEEE Transactions on*, vol. IA-22, pp. 820-827, 1986.
[21] D. Casadei, *et al.*, "FOC and DTC: two viable schemes for induction motors torque control," *IEEE Transactions on Power Electronics*, vol. 17, pp. 779-787, 2002.
[22] A. Nabae, *et al.*, "A New Neutral-Point-Clamped PWM Inverter," *IEEE Transactions on Industry Applications*, vol. IA-17, pp. 518-523, 1981.
[23] N. R. N. Idris and A. H. M. Yatim, "Direct torque control of induction machines with constant switching frequency and reduced torque ripple," *IEEE Transactions on Industrial Electronics*, vol. 51, pp. 758-767, 2004.
[24] C. L. Toh, *et al.*, "Constant and high switching frequency torque controller for DTC drives," *IEEE Power Electronics Letters*, vol. 3, pp. 76-80, 2005.
[25] A. Jidin, *et al.*, "Torque ripple minimization in DTC induction motor drive using constant frequency torque controller," in *Electrical Machines and Systems (ICEMS), 2010 International Conference on*, pp. 919-924, 2010.
[26] D. Casadei, *et al.*, "Analytical investigation of torque and flux ripple in DTC schemes for induction motors," in *Industrial Electronics, Control and Instrumentation, 1997. IECON 97. 23rd International Conference on*, vol. 2, pp. 552-556, 1997.
[27] K. J. Koo and S. S. Ki, "Torque ripple minimization strategy for direct torque control of production motor," in *Industry Applications Conference, 1998. Thirty-Third IAS Annual Meeting.* vol. 1, pp. 438-443, 1998.

[28] N. F. Alias, *et al.*, "Simple Switching Strategy for High-Torque Control Performance utilizing Neutral Point Clamped Multilevel Inverter," *International Journal of Power Electronics and Drive System (IJPEDS)*, vol. 3, pp. 400-408, 2013.

BIOGRAPHIES OF AUTHORS

Huzainirah Ismail was born in Melaka, Malaysia on 1991. She received B.Eng. degree (Hons) from Universiti Teknikal Malaysia Melaka, Malaysia in 2014 and currently pursuing M. Sc degree in the same university. Her research interests include Direct Torque Control and multilevel inverters.

Fazlli Patkar received his B.Eng and M.Eng. degree from Universiti Teknologi Malaysia, Malaysia and Ph.D. in power electronics and drives from Liverpool John Moores University, UK. Since 2014, he is a senior lecturer in Department of Power Electronics and Drives, Faculty of Electrical Engineering, Universiti Teknikal Malaysia Melaka, Malaysia. His research interest includes the power electronics converter, multiphase drive systems and DSP application on power electronics.

Auzani Jidin received his B.Eng. degree, M.Eng. degree and Ph.D. degree in power electronics and drives from Universiti Teknologi Malaysia, Johor Bahru in 2002, 2004 and 2011 respectively. He is currently a lecturer in Department of Power Electronics and Drives, Faculty of Electrical Engineering, Universiti Teknikal Malaysia Melaka, Malaysia. His research interests include the field of power electronics, motor drive systems, field-programmable gate array and DSP application.

Aiman Zakwan Jidin obtained his MEng in Electronic and Microelectronic System Engineering from ESIEE Engineering Paris France in 2011. He has 2 years of working experience in designing digital system in FPGA at Altera Corporation Malaysia, before joining Universiti Teknikal Malaysia Melaka, Malaysia as lecturer and researcher, in Electronic and Computer Engineering. His research interest includes FPGA Design and Digital System Design.

Noor Azida Noor Azlan received her B.Eng degree in Electrical Control and Instrumentation from Universiti Teknologi Malaysia (UTM) on 2011. Currently she is pursuing Msc.Eng in Electrical Science in Universiti Teknikal Malaysia Melaka, Malaysia. She has 2 years of working experience in automotive industry as Electronic Testing Engineer. Her research interest includes Direct Torque Control and Multilevel Inverter.

Tole Sutikno is an expert in the field of power electronics, industrial electronics & informatics, embedded systems and electric drives. Since 2001 he has been a lecturer in Electrical Engineering Department, Universitas Ahmad Dahlan (UAD), Indonesia. He is an Associate Professor at the above University since 2008. He received his B.Eng., M.Eng. and Ph.D degree in Electrical Engineering from Diponegoro University, Gadjah Mada University and Universiti Teknologi Malaysia, respectively. He is an Editor-in-Chief of TELKOMNIKA Telecommunication Computing Electronics and Controls, and also Editor in some international journals in electrical and computer engineering, power electronics, motor drive systems and FPGA application areas.